Structure and Properties of PBST/ZrP Nanocomposites Under the Influence of Stretching-Lamination Force Fields

Yihong Ren,[a] Huili Li,[b] and Guo Jiang [a,*]

Poly(butylene succinate-co-terephthalate) (PBST)/ layered zirconium phosphate (ZrP) composite was prepared by melt blending. The dispersion and orientation of ZrP within the PBST matrix were subsequently modified using a stretching-lamination post-treatment process. Effects of filler content and stretching ratio on the microstructure, rheological properties, thermal properties, mechanical properties, and barrier performance of the composites were investigated. Results showed that after post treatment, sliding occurred between the layers of ZrP, enhancing its dispersion within the PBST matrix and aligning it along the direction of the applied force. Furthermore, the degree of orientation increased with higher stretching ratios. In the stretching ratio of 300%, the intensity ratio of the crystal plane characteristic peaks ($I_{(002)}/I_{(100)}$) for the composite increased from 3.48 to 7.86. When the ZrP content was 3 wt% and the stretching ratio was 300%, compared with composite without post stretching, its tensile strength and elongation at break improved 10.7% and 14.4%, respectively. This study presents a novel solution to the dispersion challenges of nanofillers in composites from the perspective of processing methods, while also offering a solid foundation for the subsequent incorporation of nanocellulose to develop bio-based composites with higher mechanical strength and barrier properties.

DOI: 10.15376/biores.20.2.4346-4364

Keywords: Poly(butylene succinate-co-terephthalate); Layered zirconium phosphate; Stretching; Compression; Rheological behavior

*Contact information: a: Key Laboratory of Polymer Processing Engineering Ministry of Education, Key Laboratory of Technique and Equipment for Macromolecular Advanced Manufacturing, South China University of Technology, Guangzhou, 510640, China; b: Department of Engineering, Huzhou University, Huzhou, 313000, China; *Corresponding author: jiangguo@scut.edu.cn*

INTRODUCTION

As plastic products become increasingly widespread, the pollution and drawbacks they pose to the ecological environment are becoming more evident. Due to their high chemical stability, discarded plastic items are difficult to degrade naturally. Single-use plastics, such as bags and containers, have a short lifespan and are used frequently; their careless disposal can lead to significant environmental pollution. In recent years, there has been a growing focus on the research and application of biodegradable plastics. For example, polylactic acid (PLA) and polybutylene adipate-co-terephthalate (PBAT), as representative polymers, are extensively utilized in the processing and modification of materials (Baniasadi *et al.* 2024; Bandyopadhyay *et al.* 2024).

Poly(butylene succinate-co-terephthalate) (PBST) is a novel biodegradable aliphatic-aromatic copolyester synthesized through a polycondensation reaction using

dimethyl terephthalate (DMT) or terephthalic acid (TPA), dimethyl succinate (SA), and 1,4-butanediol (BD) as raw materials (Luo *et al.* 2010; Tsai *et al.* 2011; Lu *et al.* 2017; Wei *et al.* 2024). Because BD and SA are derived from biological fermentation, PBST is considered more environmentally friendly compared to traditional petroleum-based biodegradable polymers such as poly(butylene adipate-co-terephthalate) (PBAT) and poly(propylene carbonate) (PPC) (Lin *et al.* 2019). The PBST exhibits high elasticity and good thermal resistance; however, its relatively low water vapor barrier properties and low modulus limit its applications (Yan *et al.* 2022, 2023; Liu*et al.* 2024). To address these shortcomings and introduce new functionalities, PBST can be melt-blended with other biodegradable materials or inorganic fillers (Li *et al.* 2023; Ding *et al.* 2023).

Layered nanofillers, due to their unique two-dimensional structure, are widely used in polymer modification. Most research on blended systems involving layered nanofillers has focused on layered silicates and graphene nanosheets (Kashi *et al.* 2018; He *et al.* 2022; Wei *et al.* 2022; Zhou *et al.* 2024). However, layered zirconium phosphate (ZrP) is also one of the most important layered nanofillers, known for its excellent flame retardancy and barrier properties. Its ease of exfoliation makes it a promising candidate for enhancing the overall performance of polymers (Chen *et al.* 2021; Zhao *et al.* 2023; Mendes *et al.* 2024).

Uniaxial stretching, a common film processing method, can effectively increase the crystallinity of polymers and promote the orderly arrangement of molecular chains, thereby improving the overall performance of the final products. Multilayer stacking has also garnered attention due to its ability to enhance the mechanical properties, thermal stability, and barrier performance of film products. Both uniaxial stretching and multilayer stacking have been widely employed to enhance the performance of cellulose-based nanocomposites. Kim *et al.* (2013) demonstrated that uniaxial stretching induces highly oriented crystalline structures in cellulose films, significantly improving their thermomechanical performance with a 40% increase in storage modulus. Wang *et al.* (2024) revealed that this processing technique generates confined amorphous molecular chains within the cellulose matrix, achieving a 320% tensile strength enhancement albeit with a concomitant reduction in optical transparency to 85%. Notably, Zhu *et al.* (2024) developed a layer-by-layer laminated cellulose-silica aerogel through advanced lamination protocols, which exhibits exceptional mechanical robustness and superior thermal insulation.

Given the low tensile strength and poor barrier properties of PBST materials, this study combines uniaxial stretching with multilayer stacking techniques. Through a stretching-lamination process, the authors aimed to alter the dispersion and arrangement of layered zirconium phosphate (ZrP) fillers in the PBST matrix at varying ratios. The research investigated the effects of applying external forces during the processing of PBST/ZrP composites on their microstructure, rheological properties, mechanical performance, and barrier properties, along with a detailed mechanism analysis.

EXPERIMENTAL

Materials

The PBST (TH901T, M_W is 1.1×10^5 g mol^{-1}) used in this study was produced by Xinjiang Blue Mountain Tunhe Polyester Co., Ltd. The layered zirconium phosphate (ZrP), which has a particle size of 1 to 2 μm, was purchased from Jinda Nano Technology Co., Ltd.

Methods

The PBST and ZrP were dried in an oven at 40 °C for 24 h before use. According to the weight ratio of raw materials shown in Table 1, melt blends were performed. The mixture was subjected to melt blending in a HAAKE torque rheometer at a processing temperature of 140 °C for 6 min at a speed of 60 r/min. The resulting composite materials were then thermally pressed into sheets, which were subsequently cut into samples measuring 80 mm × 25 mm. These samples were placed in a uniaxial tensile testing machine at a constant temperature of 80 °C for tensile testing. They were held at this temperature for 2 min before being stretched to a strain of 200%. After stretching, the samples were fixed on the stretching apparatus and air-cooled to room temperature to prevent springback. The samples were then subjected to thermal pressing in groups of five. For samples with a filler content of 3 wt%, the stretching ratio was adjusted to either 100% or 300%, and the aforementioned processing steps were repeated. Untreated samples were used as the control group. The processing steps are illustrated in Fig. 1.

Table 1. Raw Material Weight Ratio and Stretching Ratio of PBST/ ZrP Composites

Sample	PBST	ZrP	Stretching Ratio (%)
PZ1	99	1	0
PZ2	98	2	0
PZ3	97	3	0
PZ5	95	5	0
PZ10	90	10	0
PZ1-200	99	1	200
PZ2-200	98	2	200
PZ3-200	97	3	200
PZ5-200	95	5	200
PZ10-200	90	10	200
PZ3-100	97	3	100
PZ3-300	97	3	300

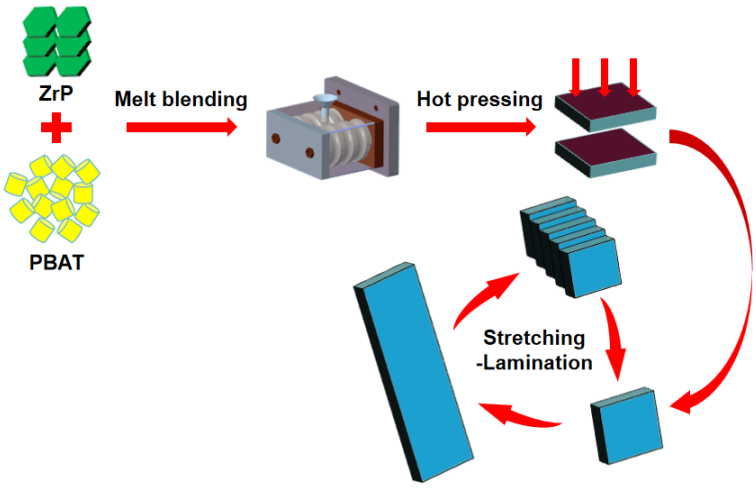

Fig. 1. Schematic diagram of the preparation process for PBST/ZrP composites

Characterization

X-ray diffraction (XRD)

The dispersion of ZrP in the composite samples before and after the stretching-lamination treatment was analyzed using a wide-angle X-ray diffractometer (WXRD D8 Advance, Bruker, Germany). The testing wavelength was set to 0.154 nm, with a scanning range of 5 to 50° and a scanning speed of 6°/min.

Scanning electron microscopy (SEM)

The prepared composite samples were immersed in liquid nitrogen for 20 min, then they were fractured to obtain brittle samples, which were subsequently gold-coated (SBC-12, KYKY, China). The surface morphology of the fractured samples was observed using a scanning electron microscope (SEM, Merlin, Zeiss) at a working voltage of 10.0 kV.

Differential scanning calorimetry (DSC)

The thermal properties of the composites were studied using DSC (DSC204, NETZSCH, Germany) under a nitrogen atmosphere. The samples to be tested were placed in an oven at 40 °C for 12 h to dry. The weight of the samples ranged between 5.0 and 10.0 mg. The films were heated from ambient temperature to 140 °C at a heating rate of 10 °C·min^{-1} and kept the temperature at 140 °C for 5 min. Then the films were cooled to 20 °C at a cooling rate of 10 °C·min^{-1}. After holding at 20 °C for 5 min, the films were reheated to 140 °C at the same heating rate of 10 °C·min^{-1}. The crystallinity (*Xc*) was calculated using the following formula (Wang *et al.* 2023),

$$X_c = \frac{\Delta H_m}{\Delta H_0} \times 100\% \quad (1)$$

where the $\triangle H_m$ and $\triangle H_0$ represent the heat of fusion of the composite and the heat of fusion of 100% crystallinity. For PBST, the $\triangle H_0$ is 145.5 J/g.

Rheological characterization

The composite materials were pressed into 1-mm-thick sheets using a plate press, from which circular discs with a diameter of 25 mm were cut out and placed in an oven at 40 °C for 12 h to dry. The rheological properties of the composites were then tested using an MCR 301 rotational rheometer (Anton Paar, Austria) in oscillation mode. The testing temperature was set to 140 °C, with a dynamic frequency scanning range of 0.01 to 100 Hz and a fixed strain of 1%.

Mechanical properties

The composite materials were pressed into 1-mm-thick sheets and then cut into dumbbell-shaped specimens for tensile testing. Prior to testing, all samples were dried in an oven at 40 °C for 12 h. The tensile tests were conducted using a universal tensile testing machine (104B, Shenzhen Wan Testing Equipment Co., Ltd., China). The testing standards followed ISO 1184 (1983) (Jiang *et al.* 2022), with a tensile rate of 50 mm/min. Each group of tests consisted of five specimens, and the average values were calculated.

Thermogravimetric analysis (TGA)

The thermal stability of the composite film samples was evaluated using a thermogravimetric analyzer (TGA209, Netzsch, Germany). The samples, weighing

between 5 to 10 mg, were tested in a nitrogen atmosphere over a temperature range of 30 to 600 °C, with a heating rate of 10 °C/min.

Water vapor permeability of the films (WVP)

The composite materials were pressed into films with a thickness of 300 μm, from which circular samples with a diameter of 60 mm were cut. Prior to testing, the samples were dried in an oven at 40 °C for 12 h, while anhydrous calcium chloride was dried in an oven at 150 °C for 3 h. The water vapor permeability of the samples was measured using a high-low temperature constant humidity chamber (GDW/JB-0150, Wuxi Nanya Technology Co., Ltd.) in accordance with GB/T 1037 (2021) (Jiang *et al.* 2024). The test was conducted at a temperature of 23 °C and a relative humidity of 90% RH for a duration of 24 h. The weight changes of the permeation cups were recorded before and after the experiment, with three samples tested per group to calculate the average value. The water vapor permeability coefficient (WVP) was calculated using the following formula (Jiang *et al.* 2022; Jiang *et al.* 2024),

$$WVP = \frac{\Delta m \cdot d}{A \cdot t \cdot P_0 \cdot RH} \quad (2)$$

where A is the permeation area of the sample (cm²), t is the time interval between the two measurements (s), P_0 is the saturation vapor pressure at the testing temperature (Pa), RH is the relative humidity (%) of the testing environment, Δm (g) is the mass increase of the permeation cup during the time period t, and d is the thickness of the sample (cm).

RESULTS AND DISCUSSION

Stretching-Lamination Treatment's Effect on the Dispersion of ZrP

Figure 2 illustrates the microstructural morphologies of the composites after treatment at different stretching ratios under conditions of low, medium, and high filler content. Figure 3 shows the structural diagram and microscopic morphology of ZrP. Prior to treatment, ZrP exhibited a random distribution within the PBST matrix, and at higher filler concentrations, agglomeration of the nanosheets was observed. At a filler content of 1 wt%, a stretching ratio of 100% was sufficient to achieve a favorable orientation effect. However, when the filler content increased to 3 wt%, a stretching ratio of 200% or higher was necessary to align the ZrP along the direction of stretching. As the filler content rose to 10 wt%, the required stretching ratio increased to 300%. This phenomenon indicates that higher filler concentrations necessitate greater stretching ratios to achieve orientation along the stretching direction. In comparison to the pre-treatment state, the post-treatment composites exhibited orientation of the ZrP, with a noticeable reduction in the stacking of nanosheets and a more uniform distribution. The structural evolution of ZrP under uniaxial stretching can be explained through coupled interfacial mechanics and energy minimization principles. The interlayer domains of ZrP, primarily connected by hydrogen bonds with relatively low binding energy, exhibit weak resistance to shear deformation. During stretching, the mechanical deformation of the PBST matrix induces interfacial shear stress transfer to ZrP interlayers, generating a non-uniform interlayer shear stress field. Once the localized shear stress surpasses the critical threshold of hydrogen bond networks, interlayer sliding initiates as the externally applied work overcomes the energy barrier. Concurrently, according to Eshelby's inclusion theory (Sidhardh and Ray 2019),

the rigid ZrP particles dispersed in the matrix create localized strain field distortion under uniaxial tension. To achieve thermodynamic equilibrium through strain energy minimization, these ZrP lamellae undergo spontaneous orientation adjustment, progressively aligning their longitudinal axes with the stretching direction. This orientation-driven restructuring effectively reduces the strain mismatch at the filler-matrix interface, ultimately forming an anisotropically reinforced composite architecture. Additionally, during the compression phase, the high temperature and pressure conditions facilitated the flow and diffusion of the polymer matrix, promoting the rearrangement and alignment of the layered fillers along the flow direction. The comparison of the dispersion structure of layered ZrP in the PBST matrix before and after treatment clearly demonstrates that the stretching-lamination process was effective in achieving the re-dispersion of two-dimensional layered fillers within the polymer matrix.

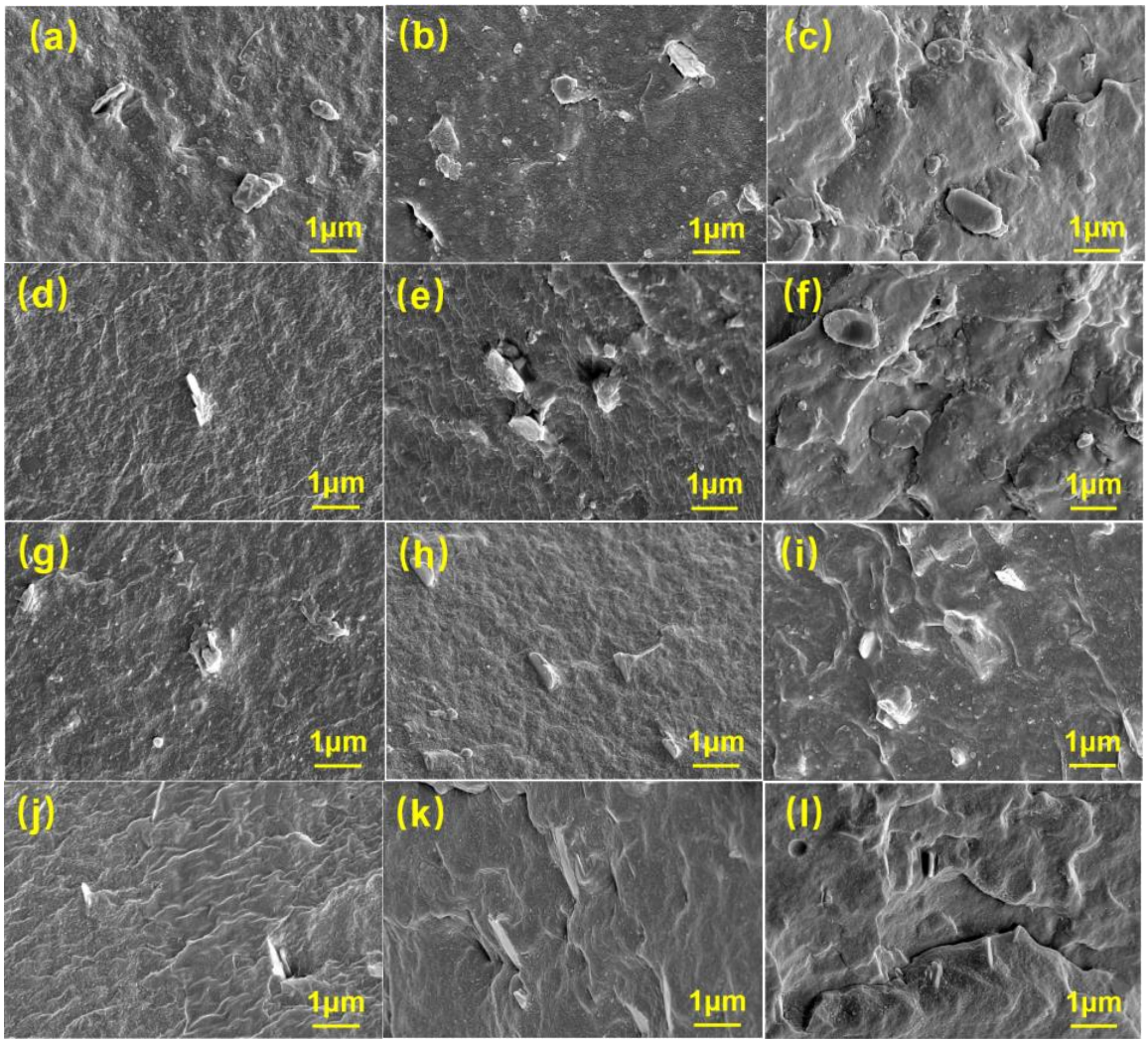

Fig. 2. Microstructures of the composites at different stretching ratios with a filler content of 1 wt%: (a) PZ1 (d) PZ1-100 (g) PZ1-200 (j) PZ1-300; Microstructures of the composites at different stretching ratios with a filler content of 3 wt%: (b) PZ3 (e) PZ3-100 (h) PZ3-200 (k) PZ3-300; Microstructures of the composites at different stretching ratios with a filler content of 10 wt%: (c) PZ10 (f) PZ10-100 (i) PZ10-200 (l) PZ10-300

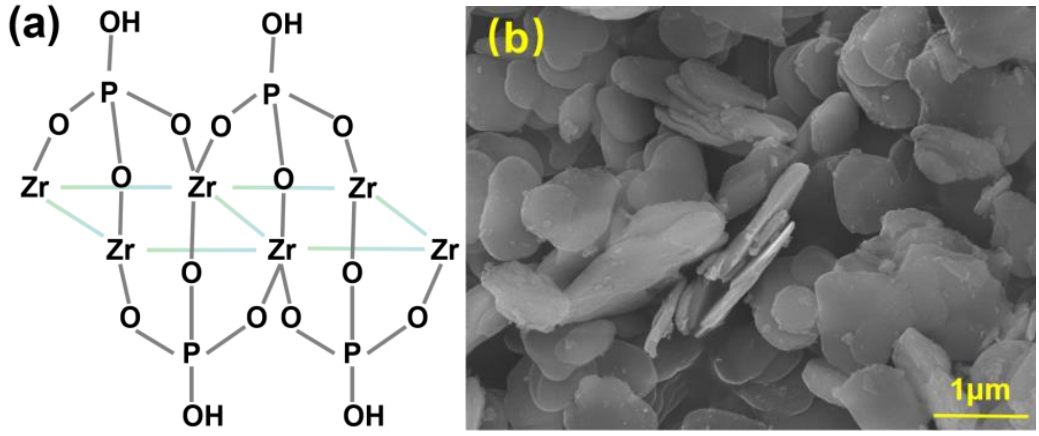

Fig. 3. (a) The structural diagram of ZrP, (b) Microscopic morphology of ZrP

XRD Analysis

As shown in Fig. 4b, the X-ray diffraction patterns of the PBST/ZrP composites with a filler content of 2 wt% before and after Stretching-Lamination treatment are presented. The diffraction peaks at approximately 11.7° and 23.2° correspond to ZrP and PBST, respectively. The intensity ratio of the two crystal planes, ($I_{(002)}/I_{(100)}$), is commonly used to indicate the orientation of ZrP within the composite; a higher ratio signifies a greater degree of orientation (Li *et al.* 2021). Before treatment, the ($I_{(002)}/I_{(100)}$) ratio was 3.48. As the tensile strain increased, the ratio began to rise, reaching 7.86 at a tensile strain of 300%, indicating a higher orientation of ZrP at this point.

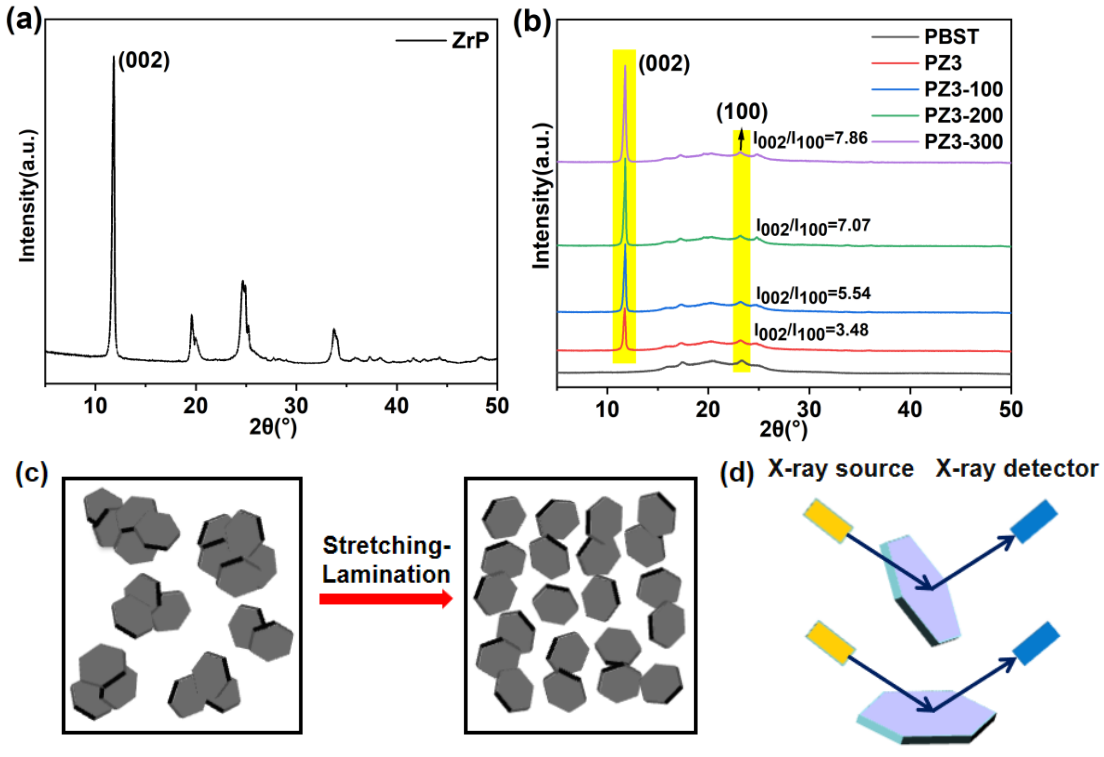

Fig. 4. (a) X-ray diffraction pattern of ZrP, (b) X-ray diffraction patterns of the composites under different stretching ratios, (c) Schematic illustration of the dispersion of ZrP, (d) Schematic representation of the diffraction of ZrP crystal planes before and after orientation

This enhancement in orientation is attributed to the reduced agglomeration of nanosheets after ZrP alignment. This reduction increases the specific surface area and alters the orientation of the crystal planes. Consequently, the increased interaction of X-ray diffraction with the crystal planes leads to an increase in the intensity of the characteristic diffraction peaks. The addition of the filler did not alter the position of the diffraction peaks for PBST, indicating that there was no reaction between PBST and ZrP. Furthermore, due to the relatively weak crystallinity of PBST, the introduction of a small amount of filler did not result in any pronounced changes to its diffraction peak positions. For further clarification, Figs. 4c and 4d illustrate the changes in the dispersion state of ZrP before and after the stretching-lamination treatment. These figures also provide a schematic representation of the crystal plane diffraction.

DSC Analysis

To investigate the influence of tensile deformation on the crystallization performance of composites, the first heating DSC curves of PBST/ZrP composites treated with different draw ratios were examined as shown in Fig. 5, with detailed crystallization parameters listed in Table 2. The PBST exhibited a crystallinity value of 6.47%, which increased to 7.65% after incorporating 3 wt% ZrP. This is due to the heterogeneous nucleation effect of ZrP, which provides additional nucleation sites and thereby reduces the free energy barrier for PBST crystallization, enhancing its crystallization ability. After stretch-lamination processing, the X_c of composites further increased and demonstrated a positive correlation with draw ratio.

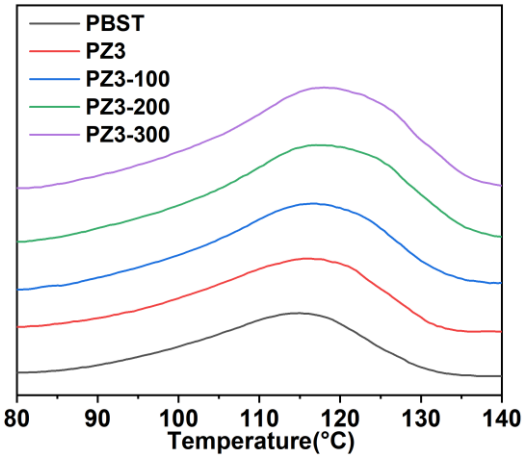

Fig. 5. DSC first heating curves of the composites under different stretching ratios

At 300% draw ratio, the crystallinity of PZ3-300 reached 9.87%, representing a 29% enhancement compared to non-stretched PZ3. This is due to the stretching-induced crystallization effect. Under high tensile deformation, the alignment of polymer chains along the stretching direction reduces interchain entanglements and conformational disorder. Such orientation imposes geometric constraints on chain mobility, thereby lowering the system entropy while promoting the formation of periodically ordered crystalline domains through localized nucleation and growth. Concurrently, tensile stress enhances the exfoliation and spatial redistribution of ZrP, which amplifies the heterogeneous nucleation efficiency by increasing the accessible surface area for polymer matrix interactions. These synergistic effects collectively elevate the crystallinity of the

composite system. A consistent trend was observed in the melting peak temperature evolution. However, since PBST is an amorphous copolymer with a crystallinity of approximately 7% (Gang *et al*. 2023), the stretching process in this experiment was found to have a relatively limited effect on the crystallinity increase of the PBST/ZrP composites. The primary effects were observed in the enhanced dispersion and orientation of the layered ZrP.

Table 2. Crystallization Parameters of the Composites under Different Stretching Ratios

Sample name	ΔH_m (J/g)	T_m (°C)	X_c (%)
PBST	9.42	114.4	6.47
PZ3	11.13	115.8	7.65
PZ3-100	12.13	116.6	8.34
PZ3-200	13.43	117.3	9.23
PZ3-300	14.36	117.7	9.87

Rheological Behavior Analysis

As shown in Fig. 6, the curves representing the relationship between η^* and frequency for the composite materials before and after stretching-lamination treatment at a strain of 200% are presented. Both η^* values decreased with increasing frequency, indicating pseudoplastic fluid behavior and shear thinning. Additionally, η^* increased with the rising content of ZrP, influenced by two main factors. On one hand, the layered filler ZrP restricts the movement of the polymer chains; on the other hand, the abundant hydroxyl groups present between the ZrP layers form hydrogen bonds with the polymer molecules, further hindering chain mobility. In the low-frequency region, the increase in η^* with higher filler content was more pronounced than in the high-frequency region. This is because higher scanning frequencies lead to more vigorous molecular chain movement, which diminishes the filler's hindering effect on chain mobility. Furthermore, for composites with the same filler content, the η^* values after stretching-lamination treatment were higher than those before treatment. This was primarily due to the reduced agglomeration of ZrP within the PBST matrix following the treatment, resulting in enhanced orientation. The increased rigidity of ZrP enhanced its ability to constrain the PBST molecular chains, thereby improving the efficiency and leading to an increase in η^*.

As shown in Figs. 6b and 6d, the relationship between G' and frequency for the PBST/ZrP composite system before and after stretching-lamination treatment is compared. The G' values for the treated composite systems were generally higher than those for the untreated systems at the same filler content. Specifically, for the composite materials with a filler content of 3 wt%, the G' curve before treatment was steeper at lower scanning frequencies, while the curve after treatment was more gradual. This indicates that the treated composite system underwent a transition from a liquid-like to a solid-like behavior. The improvement in the dispersion of the nanofiller following the stretching-lamination treatment enhanced the interfacial friction between ZrP and the PBST matrix. This enhancement facilitated the rheological percolation behavior of the composite material at

lower filler contents. The increase in *G*' suggests that both the addition of ZrP and the Stretching-Lamination treatment contributed to increasing the melt strength.

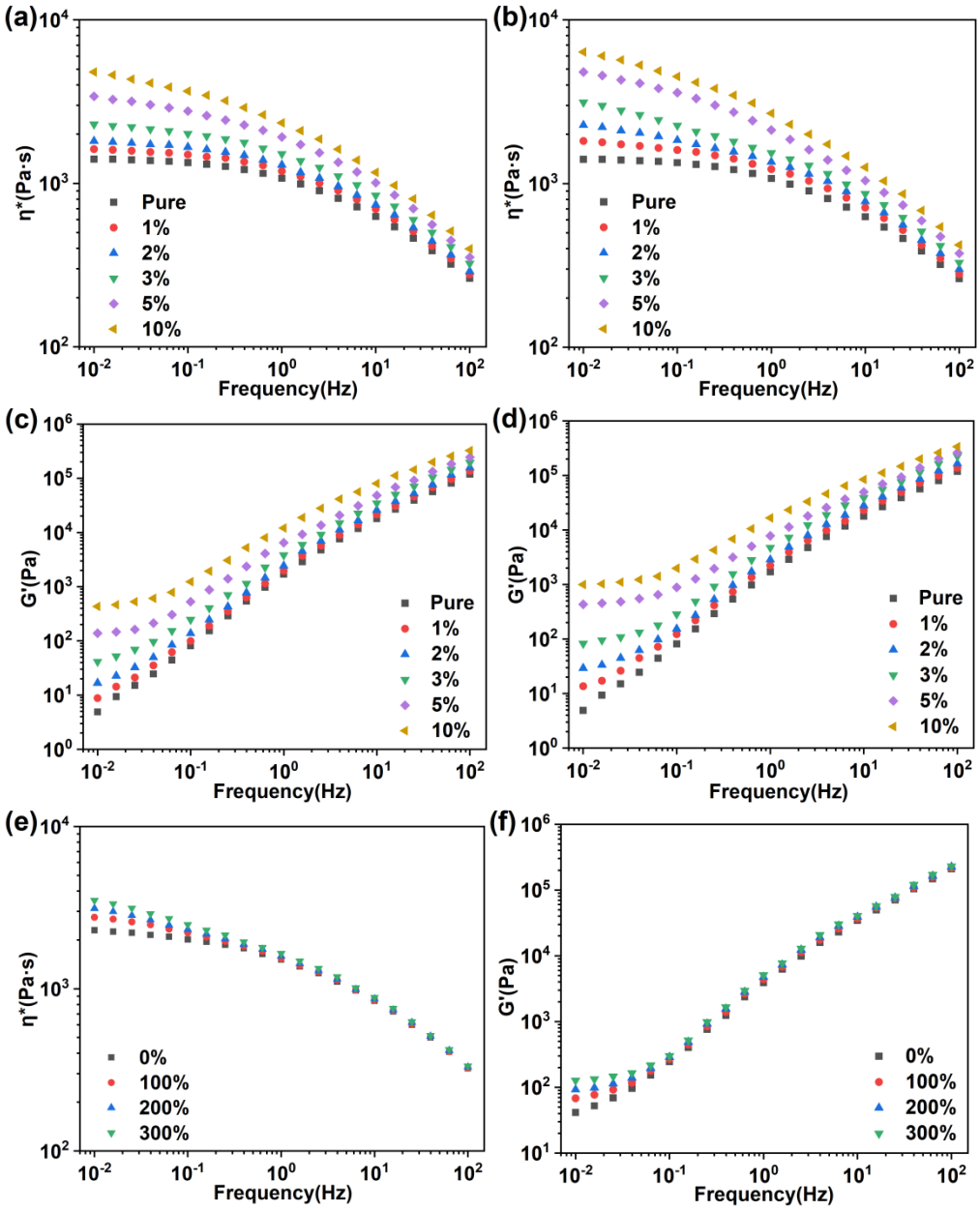

Fig. 6. Before Stretching-Lamination treatment: (a) Complex viscosity, (b) Storage modulus; After Stretching-Lamination treatment: (c) Complex viscosity, (d) Storage modulus; Different stretching ratios: (e) Complex viscosity, (f) Storage modulus

Table 3. Percolation Threshold and Critical Exponent for the Nanocomposite Samples

Sample	Percolation Threshold (φ_c)	Critical Exponent (t)
PZ	0.93	1.13
PZ-200	0.87	1.36

The results of the storage modulus at low frequencies can be used to determine the microstructure of the dispersions. To quantify the rheological percolation threshold, the following percolation model was used,

$$G_0^{'} \sim (\varphi - \varphi_c)^t \quad (3)$$

where $G_0^{'}$ represents the storage modulus at the low frequency of 0.0628, φ is the ZrP weight fraction, φ_c is that at the percolation threshold, and t is a critical exponent representing the fractal dimension of the nanoparticle 3D networks (Shih *et al.* 1990; Foudazi and Nazockdast 2013). The best linear fit of the *versus* plot was used to estimate the value of the percolation threshold and the critical exponent for the nanocomposite samples. The obtained data are summarized in Table 3. Upon comparative analysis of these results, it becomes apparent that composite materials subjected to the stretching-lamination treatment displayed a reduced rheological percolation threshold, thereby facilitating the formation of a rheological percolation network at a lower concentration of fillers.

Figures 6e and 6f illustrate the η^* and G' of the composite materials with a filler content of 3 wt% under different stretching ratios. As the tensile strain increased, η^* shows a general upward trend, with a significant increase at 200%. This indicates that a significant portion of the ZrP had become oriented along the tensile direction at this strain. However, as the tensile strain continued to increase, the rate of increase in η^* began to slow down. A similar trend was observed in G'. This suggests that at a filler content of 3 wt%, a tensile strain of 200% results in a favorable orientation distribution of ZrP.

Mechanical Properties

Figure 7a shows the mechanical properties of the PBST/ZrP composites before and after stretching-lamination treatment at a strain of 200%. Before treatment, the addition of a small amount of filler increased the tensile strength of the composites, reaching a maximum at a filler content of 2 wt%, which represents an increase of 2.3 MPa compared to pure PBST. This is because the hydroxyl groups on the surface of ZrP fillers are capable of forming hydrogen bonds with the polar groups within the PBST matrix. This interfacial interaction strengthens the adhesion between the filler and the matrix, thereby enhancing the overall mechanical properties of the composite material. However, as the filler content continued to rise, the mechanical strength began to decline due to the agglomeration of excess ZrP, leading to stress concentration. For any given filler content, the tensile strength of the composites after stretching-lamination treatment was higher than that before treatment, with the maximum increase observed at 3 wt%. At this point, the tensile strength of PZ3-200 had increased 8.9% compared to PZ3. This improvement was primarily due to the stretching-lamination treatment, which facilitated the sliding of layered ZrP along the direction of applied force, enhancing the dispersion of the filler and reducing nanoparticle agglomeration. Consequently, the reduction in stress concentration points, coupled with better dispersion, increased the interfacial friction between the ZrP filler and the PBST matrix, thereby improving the tensile properties of the composite (Tang *et al.* 2024). A similar trend was observed in the increase in elongation at break of the composites after treatment. For PZ2 and PZ3, the elongation at break increased from 1920% and 1800% to 2030% and 2010% after treatment. This further confirms the effectiveness of the Stretching-Lamination process in improving filler dispersion and reducing stress concentration.

Figure 7b shows the tensile strength and elongation at break of the PBST/ZrP with a filler content of 3 wt% under different stretching ratios. It is evident that both the tensile

strength and elongation at break of the composites increased with increasing tensile strain, reaching their maximum values at 300%. Compared to the untreated PZ3, the PZ3-300 exhibited improvements of 10.7% in tensile strength and 14.4% in elongation at break. This indicates that as the tensile strain increased, the orientation of the ZrP became more pronounced, reducing agglomeration points and enhancing dispersion.

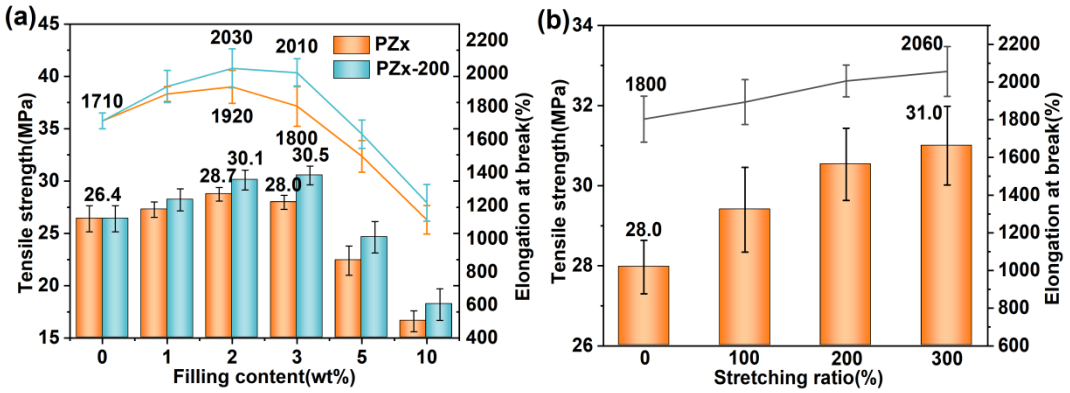

Fig. 7. Tensile strength and elongation at break: (a) Composites before and after Stretching-Lamination treatment at different filler contents, (b) Composites with a filler content of 3 wt% under different stretching ratios

Thermal Stability

Figure 8 shows the thermogravimetric (TGA) curves and the derivative thermogravimetric (DTG) curves of the composites. Table 4 lists the temperatures corresponding to various weight loss (5%, 25%, and 50%) and the maximum weight loss rates. When the maximum weight loss temperature is selected as a comparison point, the thermal decomposition temperature of the composites shows a pronounced increase with the addition of 1 wt% and 2 wt% ZrP. This phenomenon is attributed to the formation of hydrogen bonds between the hydroxyl groups on the ZrP surface and the polar moieties of PBST chains, thereby restricting the mobility of polymer chains. This restriction increases the energy barrier required for molecular chain scission during thermal decomposition, effectively elevating the activation energy of the reaction. According to the Arrhenius equation, an increase in activation energy leads to a decrease in the thermal decomposition reaction rate constant (Chen and Liu 2010). Consequently, at the same heating rate, the decomposition process is kinetically delayed, which is manifested as a notable shift of the thermal decomposition temperature to higher values. Additionally, the two-dimensional structure of the filler effectively suppresses the escape of volatile degradation products from the polymer, creating a physical shielding effect. However, as the filler content continues to increase, the thermal decomposition temperature of the composites begins to fall below that of pure PBST. This decline may be due to excessive ZrP content leading to agglomeration, which reduces the specific surface area of the filler and weakens the interactions with the matrix. This phenomenon can also create localized high-temperature regions that accelerate the thermal degradation of PBST. When $T_{5\%}$ is chosen as the comparison point, its trend mirrors that of T_{mix}. However, the decomposition temperature of the PZ10 decreases 17.7 °C compared to PBST. This reduction occurs because, within the temperature range of 100 to 400 °C, the layered ZrP undergoes a dehydration process. The evaporation of free water and crystallization water between the ZrP layers results in mass loss (Xu *et al.* 2018). At approximately 350 °C, the mass loss of ZrP is pronounced,

while PBST experiences relatively less mass loss, leading to considerable differences in the thermal decomposition temperatures of the composites with varying filler contents.

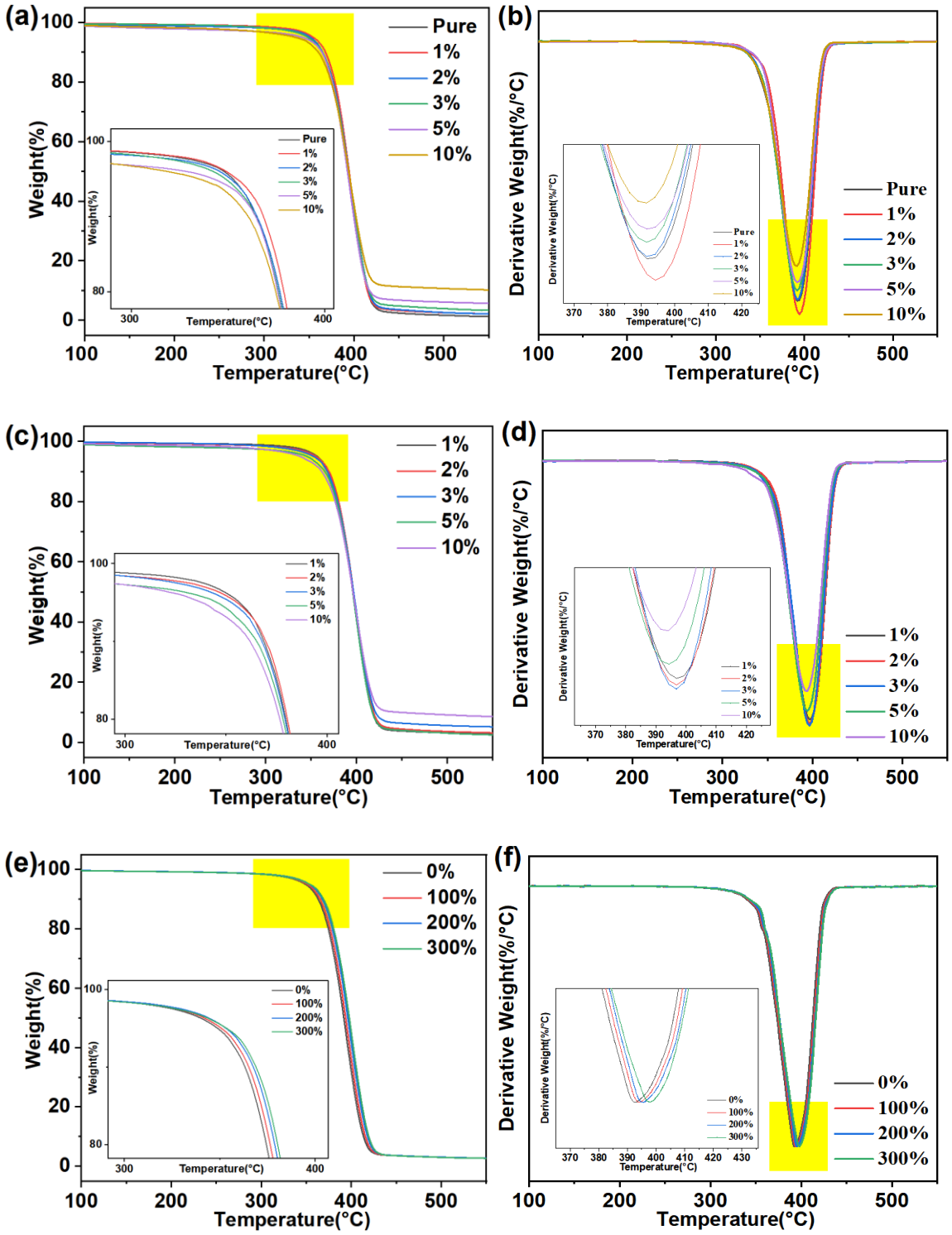

Fig. 8. Thermogravimetric (TGA) (a) and derivative thermogravimetric (DTG) (b) of PZx at different filler contents; TGA (c) and DTG (d) of PZx-200 after Stretching-Lamination treatment under different filler contents; TGA (e) and DTG (f) of the composites with a filler content of 3 wt% at different draw ratios

Table 4. Thermal Decomposition Temperatures of PBST/ZrP Composites Before and After Treatment at Different Filler Contents and Stretching Ratios

Sample	$T_{5\%}$	$T_{25\%}$	$T_{50\%}$	T_{mix}
PBST	352.5	380.6	394.2	396.2
PZ1	354.4	382.2	394.6	396.9
PZ2	351.2	380.5	394.2	396.7
PZ3	348.6	379.8	393.6	395.8
PZ5	342.5	379.3	392.7	393.5
PZ10	334.8	378.9	392.5	392.2
PZ1-200	356.3	383.2	395.9	397.4
PZ2-200	354.5	383.8	396.8	397.9
PZ3-200	352.6	382.9	396.7	397.6
PZ5-200	346.5	382.2	396.0	396.8
PZ10-200	339.0	381.1	395.3	396.1
PZ3-100	350.7	380.8	394.9	396.7
PZ3-300	353.4	383.7	397.3	398.0

After the stretching-lamination treatment, as shown in Fig. 8c, the trend in thermal decomposition temperature mirrored that of Fig. 8a. However, at the same filler content and mass loss, the thermal decomposition temperatures of the treated composites were consistently higher than those of the untreated ones. Moreover, as the filler content increased, the difference in thermal decomposition temperatures between the two conditions became more pronounced. This improvement is attributed to the stretching-lamination, which facilitated the sliding of the previously agglomerated layered ZrP, leading to a more dispersed distribution. This enhanced dispersion increased the formation of hydrogen bonds between the fillers and the PBST matrix, thereby requiring more energy to break these bonds. Additionally, better dispersion reduced the formation of localized high-temperature regions. Comparing the thermal decomposition temperatures of composites with a filler content of 3 wt% at different stretching ratios, as illustrated in Fig. 8e, it is evident that the thermal decomposition temperature increased with the tensile strain. At $T_{5\%}$, the thermal decomposition temperature of PZ3-300 was elevated by 4.8 °C compared to PZ3, and by 2.7°C compared to PZ3-100. This indicates that as the tensile strain increased, the filler achieved better dispersion.

WVP of the Composites Before and After Stretching-Lamination Treatment

Figure 9a presents the WVP of the composite films before and after the stretching-lamination treatment. As ZrP was incorporated, the WVP of the composites decreased, reaching its lowest point at a filler content of 3 wt%. At this concentration, the WVP of PZ3 was reduced by 39.4% compared to PBST. This reduction is primarily attributed to the layered structure of ZrP, which hinders the permeation of water vapor. This effectively elongates the path that water molecules must traverse through the film, thus making the permeation route more tortuous (Li *et al.* 2016). When the filler content was increased to 5 wt% and 10 wt%, the WVP slightly increased compared to the 3 wt%. This is attributable to excessive filler leading to pronounced agglomeration, which negatively impacted the tortuosity of the permeation path. After the stretching-lamination treatment, the WVP of PBST/ZrP films at the same filler content showed a marked decrease compared to the

untreated samples. This improvement is due to better dispersion, which made the path for water vapor to pass through the film more convoluted than when the fillers were agglomerated. Additionally, the oriented layered fillers aligned in the horizontal direction increase the likelihood of blocking water molecules compared to a random distribution. At a ZrP content of 3 wt% and a tensile strain of 200%, the WVP of PZ3-200 is reduced 24% compared to PZ3 and 54% compared to PBST. As shown in Fig. 9b, comparing the WVP of composite films with 3 wt% filler content after different stretching ratios, it is evident that the WVP decreases with increasing tensile strain, reaching its lowest value at a strain of 300%. At this point, the WVP is reduced 28.4% compared to the untreated PZ3. Figure 9c illustrates the permeation paths of water molecules when the fillers are arranged horizontally *versus* when they are distributed randomly, visually demonstrating the impact of ZrP orientation on the permeation pathways of water molecules.

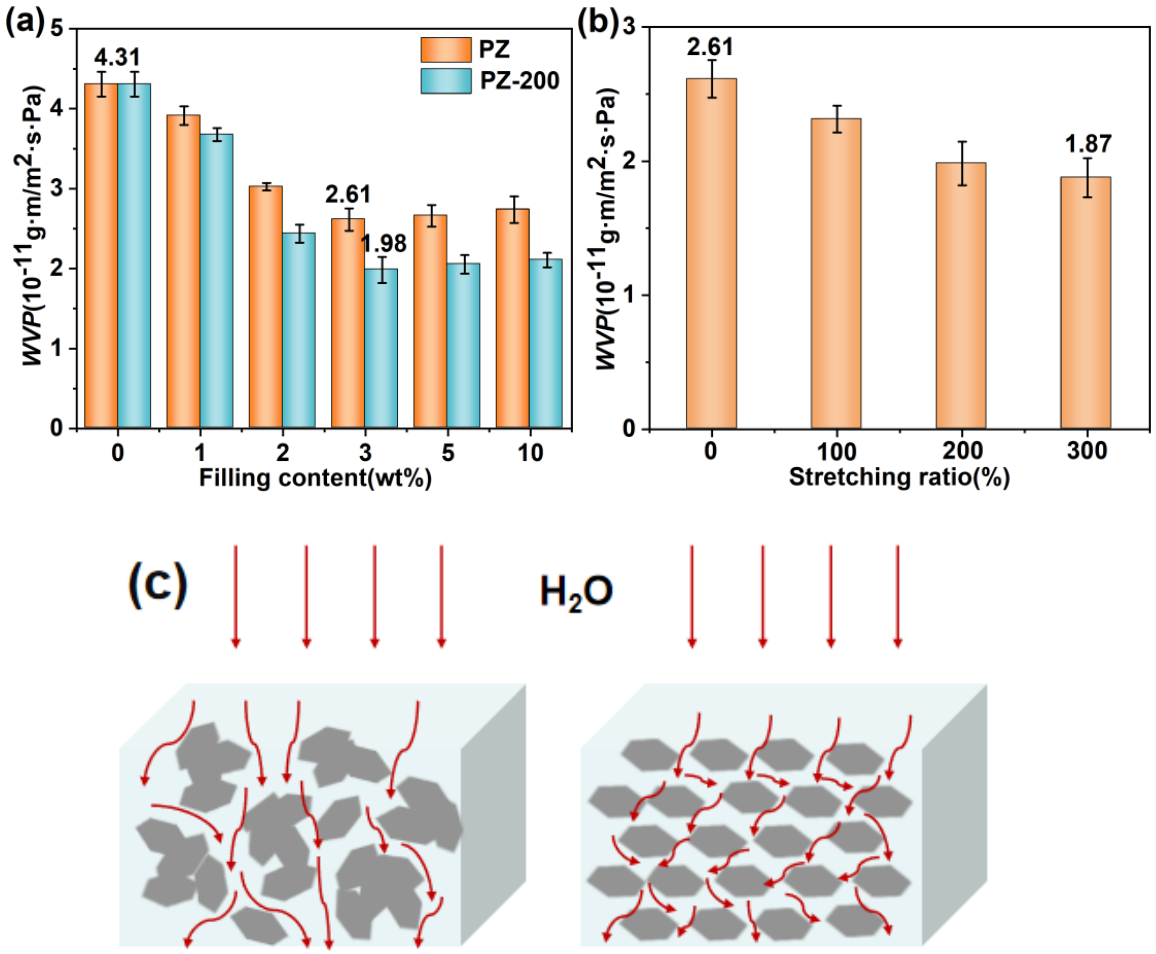

Fig. 9. (a) WVP of PBST/ZrP films before and after stretching-lamination treatment at different filler contents, (b) WVP of films treated at different stretching ratios with a filler content of 3 wt%, (c) Theoretical model of water vapor molecule permeation through PBST/ZrP films with different filler orientations

CONCLUSIONS

1. This work employed a stretching-lamination treatment to modify the structure of poly(butylene succinate-co-terephthalate (PBST) composites filled with layered zirconium phosphate (ZrP). The focus was on examining the influence of filler content and stretching ratio on the structural characteristics and performance of the resulting blends. After the stretching-lamination treatment, the dispersion of ZrP in the PBST matrix was improved, and orientation was induced along the direction of the applied force.
2. Higher stretching ratios led to better dispersion and orientation effects. Compared to the untreated samples, the rheological percolation threshold of the PZ-200 blend was reduced from 0.93 to 0.87 following the treatment process. XRD analysis revealed a pronounced enhancement in the ($I_{(002)}/I_{(100)}$) ratio, which was observed for the PZ2-300 (7.86) relative to pure PZ2 (3.48).
3. The stretching-lamination treatment enhanced the mechanical and barrier properties of the composites. The tensile strength and elongation at break of PZ3-300 increased 10.7% and 14.4% compared to PZ3, and 17.4% and 20.5% compared to PBST, respectively. Furthermore, the WVP decreased 28.4% and 56.6% compared to PZ3 and PBST.
4. It is planned to substitute ZrP with nanocellulose in subsequent investigations, employing a stretching-lamination treatment to optimize the dispersion uniformity of 1D fillers within composite matrices. Furthermore, the synergistic effects of cellulose/ZrP hybrid fillers on the comprehensive performance of resultant composites will be systematically investigated.

REFERENCES CITED

Bandyopadhyay, J., Botlhoko, O. J., Mphahlele, C., Lekalakala, R., Muniyasamy, S., and Ray, S. S. (2024). "Reactively processed poly(butylene adipate terephthalate) composite–based multilayered films with improved properties for sustainable packaging applications: Structural characterization and biodegradation mechanism," *Macromolecular Chemistry and Physics* 225(18), article 2400067. DOI: 10.1002/macp.202400067

Baniasadi, H., Äkräs, L., Madani, Z., Silvenius, F., Fazeli, M., Lipponen, S., Vapaavuori, J., and Seppälä, J. (2024). "Development and characterization of polylactic acid/ starch biocomposites – From melt blending to preliminary life cycle assessment," *International Journal of Biological Macromolecules* 279, article ID 135173. DOI: 10.1016/j.ijbiomac.2024.135173

Chen, H., and Liu, N. (2010). "Application of non-Arrhenius equations in interpreting calcium carbonate decomposition kinetics: Revisited," *Journal of the American Ceramic Society* 93(2), 548-553. DOI: 10.1111/j.1551-2916.2009.03421.x

Chen, Y., Li, J., Lai, X., Li, H., and Zeng, X. (2021). "N-alkoxyamine-containing macromolecular intumescent flame-retardant-decorated ZrP nanosheet and their synergism in flame-retarding polypropylene," *Polymers for Advanced Technologies* 32(9), 3804-3816. DOI: 10.1002/pat.5402

Ding, Y., Yu, W., Zhang, J., Liu, W., Zhu, F., Ye, Y., and Zheng, Q. (2023). "Enhanced antibacterial properties of poly(butylene succinate-co-terephthalate)/Ag@MgO nanocomposite films for food packaging," *Polymer Testing* 128, article ID 108230. DOI: 10.1016/j.polymertesting.2023.108230

Foudazi, R., and Nazockdast, H. (2013). "Rheology and morphology of nanosilica-containing polypropylene and polypropylene/liquid crystalline polymer blend," *Journal of Applied Polymer Science* 128(6), 3501-3511. DOI: 10.1002/app.38269

Gang, M., Wang, Y., Zhang, Y., Liu, L., and Shi, Y. (2023). "The relationship between microstructure and mechanical properties of PBST two-component crystalline random copolymers with different BT contents," *Polymers* 15(2), article 383. DOI: 10.3390/polym15020383

GB/T 1037 (2021). "Test method for water vapor transmission of plastic film and sheet -- Desiccant method and water method," Standardization Administration of China, Beijing, China.

He, H., Liu, B., Xue, B., and Zhang, H. (2022). "Study on structure and properties of biodegradable PLA/PBAT/organic-modified MMT nanocomposite," *Journal of Thermoplastic Composite Materials* 35(4), 503-520. DOI: 10.1177/0892705719890907

ISO 1184 (1983). "Plastics — Determination of tensile properties of films," International Organization of Standardization, Geneva, Switzerland.

Jiang, G., Wang, S., and Ren, Y. (2024). "Effect of layered double hydroxide and its localization on the structure and properties of PBAT/PPC composites," *Macromolecular Chemistry and Physics* 225(16), article 2400078. DOI: 10.1002/macp.202400078

Jiang, G., Wang, H., Yu, L., and Li, H. (2022). "Improving crystallization properties of PBSA by blending PBS as a polymeric nucleating agent to prepare high-performance PPC /PBSA /AX8900 blown films," *Polymer Engineering & Science* 62(4), 1166-1177. DOI: 10.1002/pen.25915

Kashi, S., Gupta, R. K., Kao, N., Hadigheh, S. A., and Bhattacharya, S. N. (2018). "Influence of graphene nanoplatelet incorporation and dispersion state on thermal, mechanical and electrical properties of biodegradable matrices," *Journal of Materials Science & Technology* 34(6), 1026-1034. DOI: 10.1016/j.jmst.2017.10.013

Kim, J. W., Park, S., Harper, D. P., and Rials, T. G. (2013). "Structure and thermomechanical properties of stretched cellulose films," *Journal of Applied Polymer Science* 128(1), 181-187. DOI: 10.1002/app.38149

Li, C., Wang, B., Shang, Z., Yu, L., Wei, C., Wei, Z., Sang, L., and Li, Y. (2023). "High-barrier poly(butylene succinate-co-terephthalate) blend with poly(lactic acid) as biodegradable food packaging films," *Industrial & Engineering Chemistry Research* 62(18), 7250-7261. DOI: 10.1021/acs.iecr.3c00158

Li, G., Luo, W., Xiao, M., Wang, S., and Meng, Y. (2016). "Biodegradable poly(propylene carbonate)/layered double hydroxide composite films with enhanced gas barrier and mechanical properties," *Chinese Journal of Polymer Science* 34(1), 13-22. DOI: 10.1007/s10118-016-1720-9

Li, J., Leng, J., Jiang, Y., and Zhang, J. (2021). "Experimental characterization of 3D printed PP/h-BN thermally conductive composites with highly oriented h-BN and the effects of filler size," *Composites Part A: Applied Science and Manufacturing* 150, article ID 106586. DOI: 10.1016/j.compositesa.2021.106586

Lin, S., Wang, J., Wang, H., and Wu, T. (2019). "Synthesis, mechanical properties and biodegradation of various acrylic acid-grafted poly(butylene succinate-co-terephthalate)/organically modified layered zinc phenylphosphonate nanocomposites," *European Polymer Journal* 116, 1-8. DOI: 10.1016/j.eurpolymj.2019.03.061

Liu, C., Chen, L., Yan, X., Dong, X., Tian, H., Pan, H., Wang, D., Zhao, Y., and Zhang, H. (2024). "Sustainable and biodegradable poly(butylene succinate-co-terephthalate)/ poly(propylene carbonate) blown films with enhanced compatibility, mechanical, and barrier properties," *Journal of Applied Polymer Science* 141(7), article ID e54939. DOI: 10.1002/app.54939

Lu, J., Wu, L., and Li, B. G. (2017). "Long chain branched poly(butylene succinate-co-terephthalate) copolyesters using pentaerythritol as branching agent: Synthesis, thermo-mechanical, and rheological properties," *Journal of Applied Polymer Science* 134(9), article ID 44544. DOI: 10.1002/app.44544

Luo, S., Li, F., Yu, J., and Cao, A. (2010). "Synthesis of poly(butylene succinate-co-butylene terephthalate) (PBST) copolyesters with high molecular weights *via* direct esterification and polycondensation," *Journal of Applied Polymer Science* 115(4), 2203-2211. DOI: 10.1002/app.31346

Mendes, L. C., Mariano, D. M., Freitas, D. F. S., Albitres, G. A. V., Tavares, M. I. B., and Garcia, E. E. (2024). "Ecofriendly composites based on poly (lactic acid) with nano-zirconium phosphate and nano-zinc oxide/zirconium phosphate: Physicochemical and aging characteristics," *Journal of Thermal Analysis and Calorimetry* 149(17), 9297-9306. DOI: 10.1007/s10973-024-13541-6

Shih, W. H., Shih, W. Y., Kim, S. I., Liu, J., and Aksay, I. A. (1990). "Scaling behavior of the elastic properties of colloidal gels," *Physical Review A: Atomic, Molecular, and Optical Physics* 42(8), 4772-4779. DOI: 10.1103/physreva.42.4772

Sidhardh, S., and Ray, M. C. (2019). "Size-dependent Eshelby's ellipsoidal inclusion problem based on generalized first strain gradient elasticity theory," *Mathematics and Mechanics of Solids* 24(7), 2251-2273. DOI: 10.1177/1081286518820901

Tang, S., Li, J., Li, Z., Chen, Z., Lin, J., Zhang, L., and He, S. (2024). "Enhanced mechanical properties of rubber/clay nanocomposite via compounding butadiene-styrene-vinyl pyridine rubber-contained clay gel with styrene butadiene rubber," *Polymer* 312, article ID 127643. DOI: 10.1016/j.polymer.2024.127643

Tsai, P., Wang, C., Kan, L., and Chen, C. W. (2011). "Studies on the optimal conditions for synthesizing poly(butylene succinate-co-terephthalate) copolyesters with targeted properties," *Asia-Pacific Journal of Chemical Engineering* 7(S1), S88-S94. DOI: 10.1002/apj.645

Wang, J., Chen, S., Li, D., Zhou, L., Ren, J., Jia, L., Zhong, G., Huang, H., and Li, Z. (2024). "Structuring restricted amorphous molecular chains in the reinforced cellulose film by uniaxial stretching," *Carbohydrate Polymers* 337, article 122088. DOI: 10.1016/j.carbpol.2024.122088

Wang, X., Pan, H., Jia, S., Lu, Z., Han, L., and Zhang, H. (2023). "Mechanical properties, thermal behavior, miscibility and light stability of the poly(butylene adipate-co-terephthalate)/poly(propylene carbonate)/polylactide mulch films," *Polymer Bulletin* 80(3), 2485-2501. DOI: 10.1007/s00289-022-04173-7

Wei, S., Xie, J., Zhang, J., Zhao, L., and Hu, D. (2024). "Green preparation of poly (butylene succinate-co-butylene terephthalate) foam with tunable degradability and

mechanical properties by supercritical CO_2," *Polymer Degradation and Stability* 223, article 110732. DOI: 10.1016/j.polymdegradstab.2024.110732

Wei, X., Cui, W., Zheng, K., Wang, J., Hu, J., and Zhou, H. (2022). "Bimodal cellular structure evolution in PBAT foams incorporated by carbon nanotubes and graphene nanosheets," *Journal of Polymers and the Environment* 30(7), 2785-2799. DOI: 10.1007/s10924-022-02384-7

Xu, B., Xu, W., Liu, Y., Chen, R., Li, W., Wu, Y., and Yang, Z. (2018). "Surface modification of α-zirconium phosphate by zeolitic imidazolate frameworks-8 and its effect on improving the fire safety of polyurethane elastomer," *Polymers for Advanced Technologies* 29(11), 2816-2826. DOI: 10.1002/pat.4404

Yan, X., Liu, C., He, L., Li, C., Wang, D., Wu, G., Bian, J., Zhao, Y., and Zhang, H. (2023). "Biodegradable blends of poly(butylene succinate-co-terephthalate) and stereocomplex polylactide with enhanced rheological, mechanical properties, heat resistance and hydrolytic degradation," *Journal of Materials Science* 58(14), 6391-6404. DOI: 10.1007/s10853-023-08415-5

Yan, X., Xie, R., Pan, H., Zhao, T., Han, L., Bian, J., Yang, H., Zhao, Y., Wu, G., and Zhang, H. (2022). "Effect of 1,4-bis(tert-butyl peroxy isopropyl) benzene on the rheological, mechanical, thermal and barrier properties of poly(butylene succinate-co-terephthalate)/poly(lactic acid) blends and blown films," *Materials Today Communications* 31, article 103830. DOI: 10.1016/j.mtcomm.2022.103830

Zhao, M., Wu, H., Chen, H., Lai, G., Zhu, Z., Wu, J., Kang, W., and Sue, H. (2023). "Preparation of polyethylene/α-zirconium phosphate nanocomposites *via* a well-controlled polyethylene-grafted interface," *Langmuir* 39(16), 5803-5813. DOI: 10.1021/acs.langmuir.3c00058

Zhou, S., Zhang, D., Xiong, S., Liu, Q., Shen, X., Yu, S., Sun, Z., Wen, J., Wang, L., and Yuan, T. (2024). "A high-performance and cost-effective pbat/montmorillonite/lignin ternary composite film for sustainable production," *ACS Sustainable Chemistry & Engineering* 12(40), 14704-14715. DOI: 10.1021/acssuschemeng.4c04620

Zhu, L., Shim, J., Huang, Y., Armstrong, J. N., Meng, T., and Ren, S.(2024). "Nacre-inspired hybrid multilayer insulation composites," *ACS Applied Materials & Interfaces* 16(40), 54467-54474. DOI: 10.1021/acsami.4c12012

Article submitted: February 25, 2025; Peer review completed: April 6, 2025; Revised version received: April 8, 2025; Accepted: April 14, 2025; Published: April 22, 2025.
DOI: 10.15376/biores.20.2.4346-4364